Supporting Information

Stepwise rapid electrolytic synthesis of graphene oxide for efficient adsorption of organic pollutants

Wanzhen Xu,[a] Wenjie Zhu,[a] Junliang Shen,[b] Mingyue Kuai,[b] Yi Zhang,[a] Weihong Huang,[a] Wenming Yang,*[b] Mengmeng Li*[c,d] and Sheng Yang*[e]

[a]School of Emergency Management, School of the Environment and Safety Engineering, Jiangsu University, Zhenjiang 212013, China

[b]School of Materials Science and Engineering, Jiangsu University, Zhenjiang 212013, China. E-mail: ywm@ujs.edu.cn

[c]Key Laboratory of Microelectronic Devices and Integrated Technology, Institute of Microelectronics, Chinese Academy of Sciences, Beijing 100029, China. E-mail: limengmeng@ime.ac.cn

[d]University of Chinese Academy of Sciences, Beijing 1 00049, China

[e]Frontiers Science Center for Transformative Molecules, School of Chemistry and Chemical Engineering, Shanghai Jiao Tong University, Shanghai 200240, China. E-mail: sheng.yang@sjtu.edu.cn

Results and discussion

Layer spacing calculation (XRD)

Using Bragg equation formula $2d\sin\theta=\lambda$ (where d is the crystal plane spacing, θ is

the grazing angle, λ= 0.15418 nm), it can be calculated that the spacing of EGO and HGO layers are 0.83 and 0.78 nm respectively, which is significantly larger than that of graphite (0.34 nm).

Study on adsorption isotherms and kinetics

The fitted standard curve has a high regression coefficient value (R^2=0.9993), and the absorbance value increases linearly with the increase of MB concentration. This allows us to use the standard curve of MB to accurately determine the concentration of MB during adsorption.

We use formulas (1), (2) and (3) to calculate the adsorption capacity at time t (q_t), the adsorption capacity at equilibrium (q_e) and the removal rate (R) of GO for MB.

$$q_t = \frac{(\rho_0 - \rho_t)}{m} \times V \qquad (1)$$

$$q_e = \frac{(\rho_0 - \rho_e)}{m} \times V \qquad (2)$$

$$R = \frac{(\rho_0 - \rho_e)}{\rho_0} \times 100\% \qquad (3)$$

where:

q_t - the adsorption capacity at time t / (mg g^{-1});

q_e - the adsorption capacity at equilibrium/ (mg g^{-1});

R- removal rate/ (%);

ρ_0- initial mass concentration of MB aqueous solution before adsorption / (mg L^{-1});

ρ_t- mass concentration of MB aqueous solution at time t / (mg L^{-1});

ρ_e- mass concentration of MB aqueous solution at adsorption equilibrium / (mg L^{-1});

V- volume of MB aqueous solution /L;

m- mass of adsorbent GO /mg.

Among the isotherm equations described in the adsorption of solid-liquid system, Langmuir and Freundlich adsorption isotherms are the most commonly used, which can accurately evaluate the relationship and principle of solid-liquid adsorption thermodynamics. The Langmuir isotherm model assumes that the adsorption active center energy on the solid surface is similar and uniformly distributed, and the surface adsorption is a monolayer adsorption; the Freundlich isotherm model considers the relationship between the adsorption free energy and the adsorption fraction, and is used to describe the surface inhomogeneous adsorption or surface adsorption. After adsorption of adsorbates, there is an interaction of adsorption behaviors with each other. The Langmuir and Freundlich model equations are (4) and (5), respectively:

$$\frac{C_e}{q_e} = \frac{C_e}{q_m} + \frac{1}{q_m k_L} \qquad (4)$$

$$\mathrm{Ln}\, q_e = \mathrm{Ln}\, k_F + \frac{1}{n} \mathrm{Ln}\, C_e \qquad (5)$$

where, C_e is the equilibrium concentration of MB, mg L^{-1}; q_m is the saturated adsorption capacity of the monolayer, mg/g; k_L is the Langmuir adsorption equilibrium constant; k_F and n are the adsorption coefficients of Freundlich.

Fig. S8 a-b are the linear regression curves of Langmuir and Freundlich equations obtained by plotting C_e/q_e - C_e and Ln q_e - Ln C_e, respectively. The linear fitting results are shown in Table S3. The R^2 of the Langmuir fit equation is equal to 1, which is much better than the R^2 value of the Freundlich adsorption model (0.6942). Therefore, it is more accurate to describe the adsorption of MB by EGO with the Langmuir adsorption isotherm model, indicating that the adsorption of MB by EGO is a monolayer adsorption.

In order to further illustrate the adsorption mechanism of MB on EGO, the pseudo-first-order kinetic equation (6) and pseudo-second-order kinetic equation (7) were used to study the kinetics of the adsorption of MB on EGO.

$$\frac{1}{q_t} = \frac{k_1}{q_e t} + \frac{1}{q_e} \qquad (6)$$

$$\frac{t}{q_t} = \frac{1}{k_2 q_e^2} + \frac{t}{q_e} \qquad (7)$$

where: k_1 and k_2 are the rate constants of the pseudo-first-order kinetic equation and pseudo-second-order kinetic equation, respectively; q_t and q_e are the adsorption amount (mg g^{-1}) of MB on EGO at the adsorption time t and when the adsorption reaches equilibrium, respectively.

The experimental data of MB with a concentration of 10 mg L^{-1} were selected and substituted into the kinetic formula for linear fitting (Fig. S9 a-b), and q_e, R^2, k_1 and k_2 were calculated respectively (Table S4). It can be seen that the correlation of the pseudo-first-order kinetic fitting curve is low, while the pseudo-second-order kinetic fitting curve shows a good linear relationship. The R^2 in the pseudo-first-order adsorption kinetic model is 0.8044, while the R^2 in the pseudo-second-order adsorption kinetic model is 0.9990. The theoretical adsorption capacity (366 mg g^{-1}) calculated by the pseudo-second-order adsorption kinetic model is better than and close to the actual value of 358 mg g^{-1}. So, the adsorption of MB by EGO is more in line with the pseudo-second-order adsorption kinetic model.

Supplementary Figures

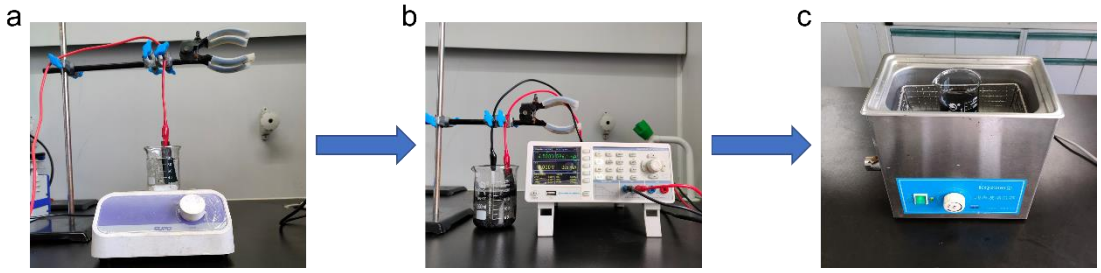

Fig. S1 Process for preparing EGO: a, intercalation of CGF in $(NH_4)_2S_2O_8$-H_2SO_4 solution; b, exfoliation of the GICs in 50 wt.% H_2SO_4 at +4.5 V; c, sonication of the EGO in water.

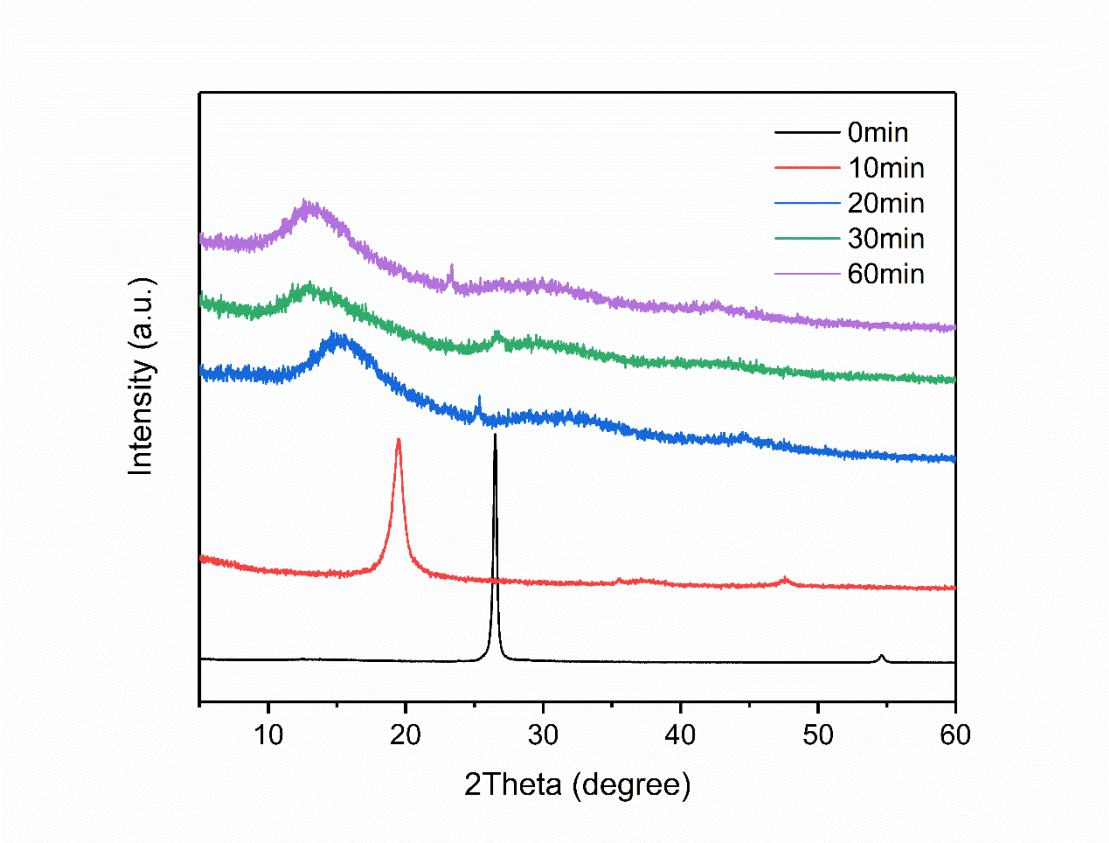

Fig. S2 XRD patterns of the first step (intercalation) at different reaction times.

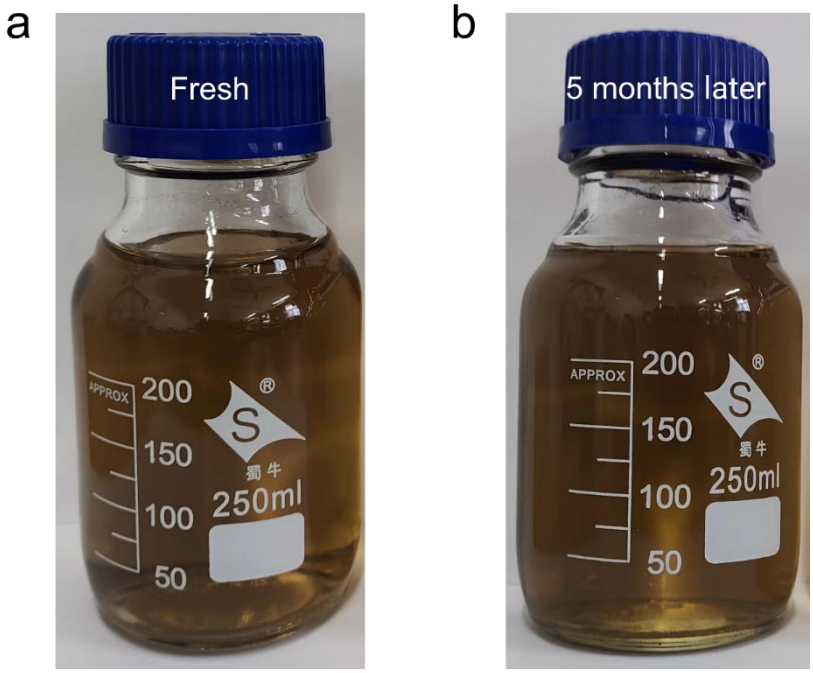

Fig. S3 Comparison of color change of EGO aqueous solution (0.05mg mL^{-1}) before and after the storage for five months.

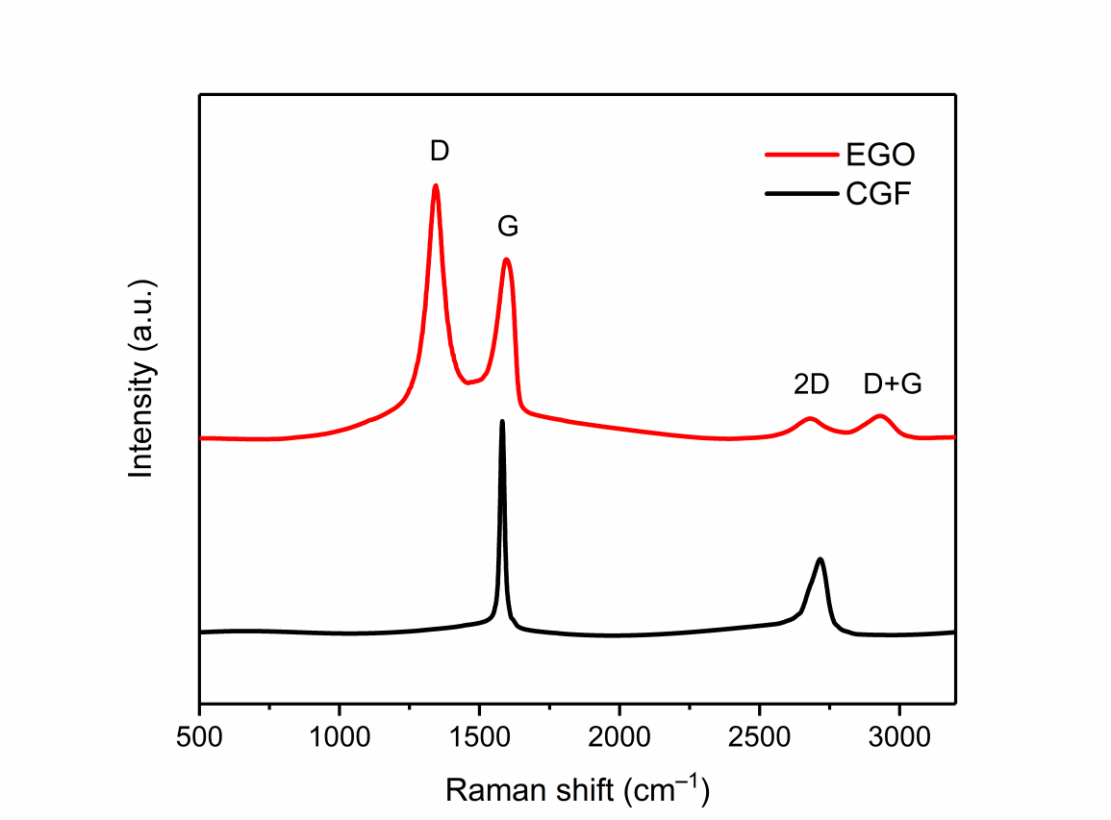

Fig. S4 Raman spectra of the EGO and CGF.

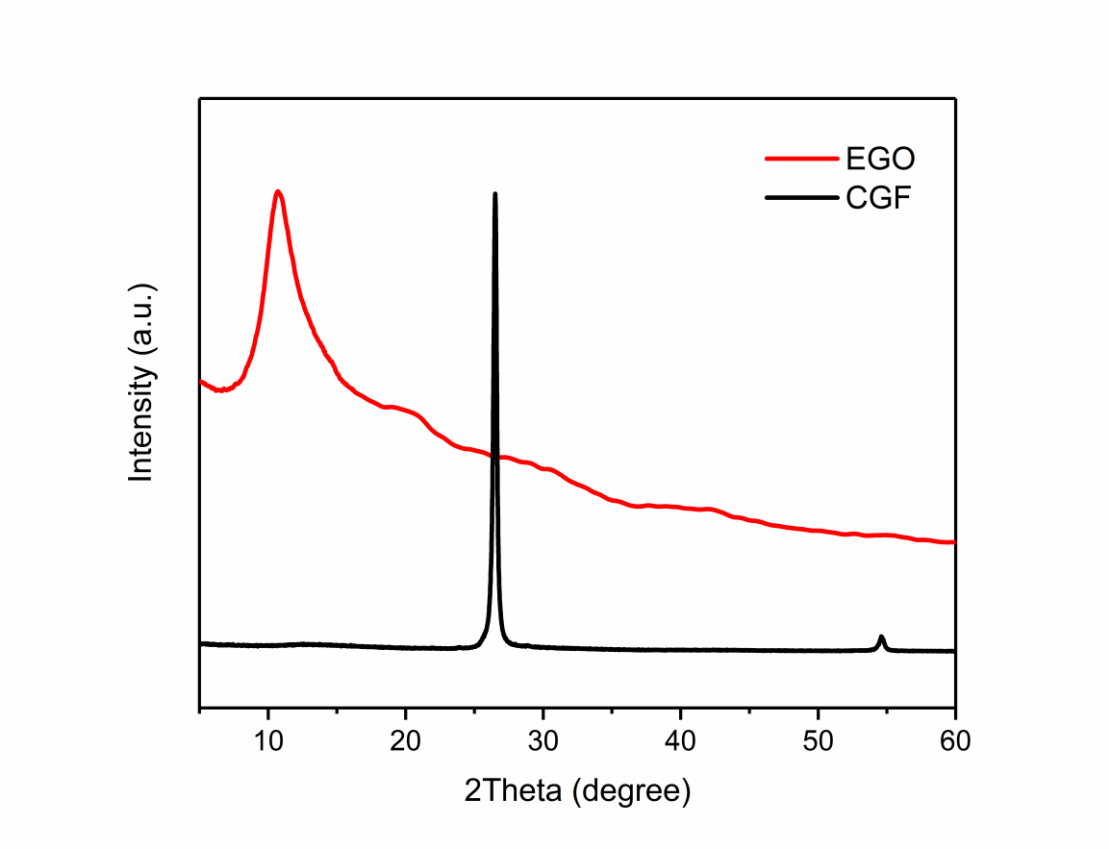

Fig. S5 XRD patterns of the EGO and CGF.

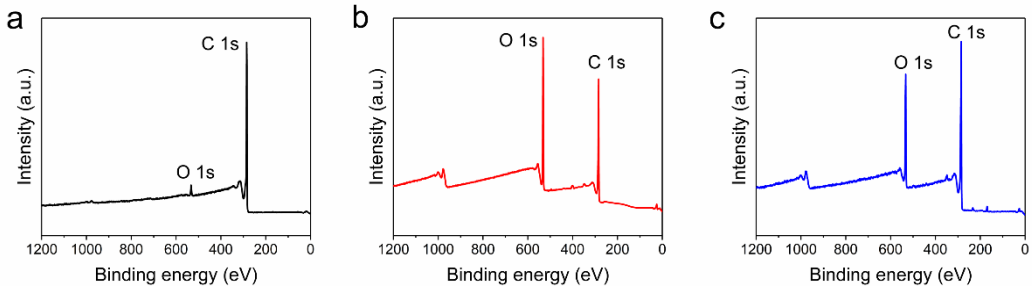

Fig. S6 XPS survey spectra of: a) CGF (oxygen content of 2.7 at.%); b) EGO (oxygen content of 33.7 at.%); c) HGO (oxygen content of 17.4 at.%).

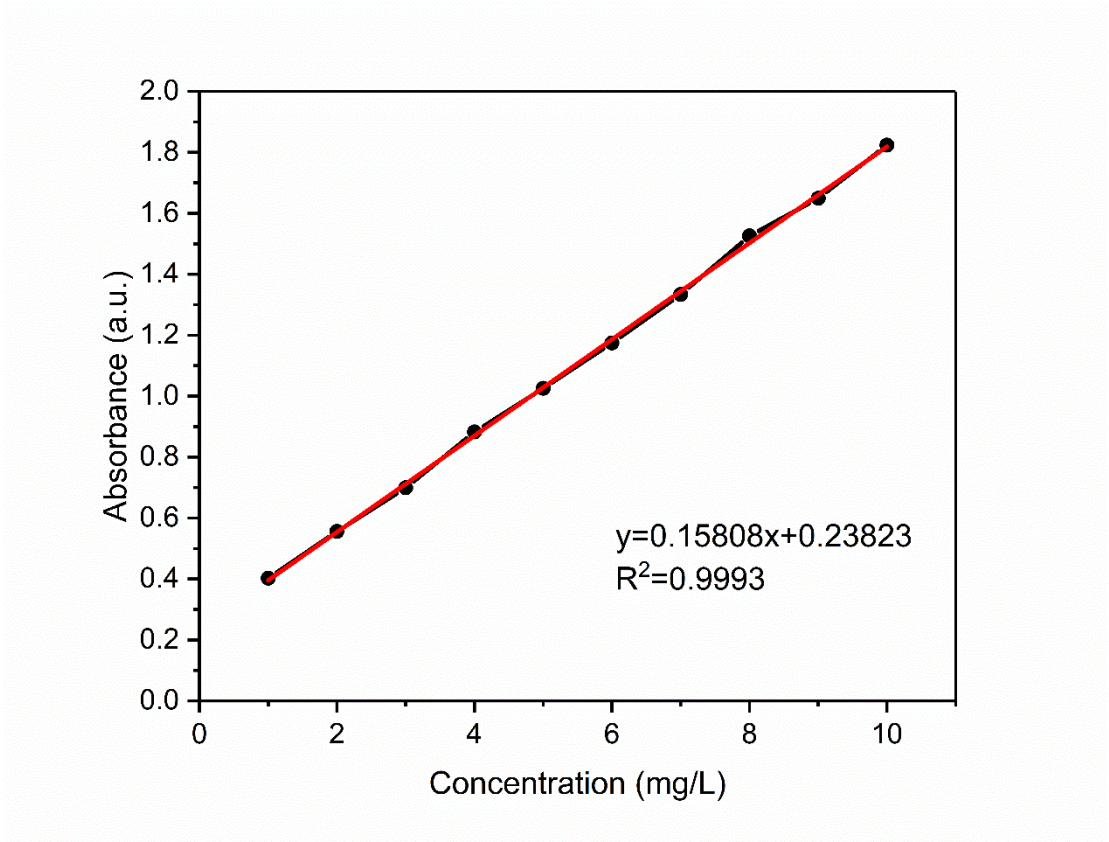

Fig. S7 Calibration curve for concentration of MB dye solution.

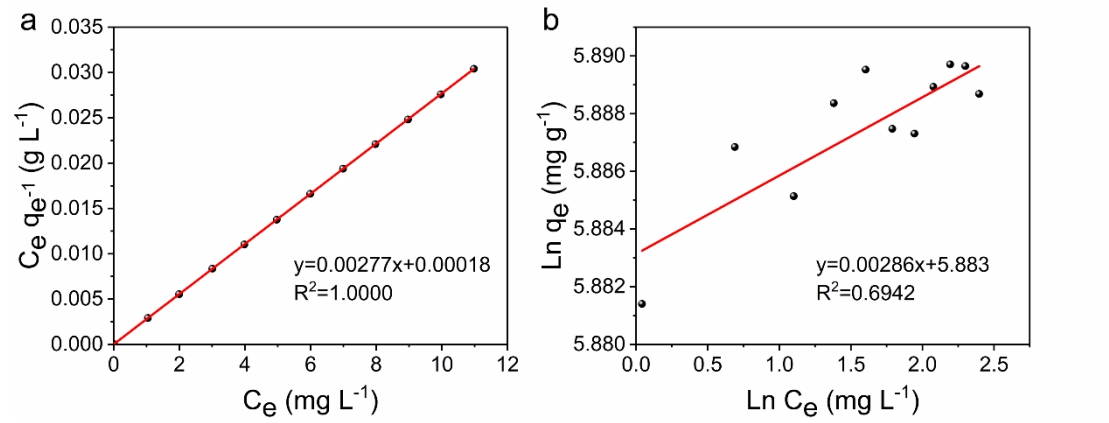

Fig. S8 Langmuir(a) and Freundlich(b) isotherms for MB dye onto EGO.

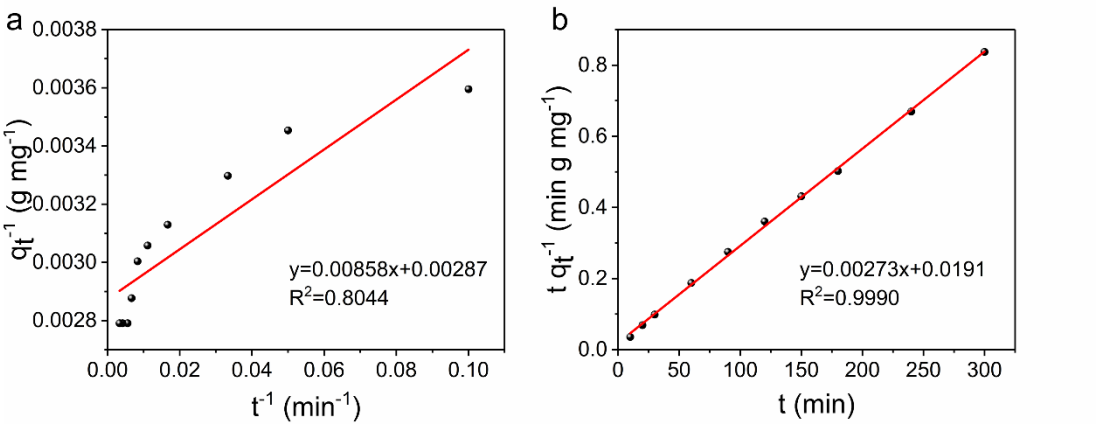

Fig. S9 Pseudo-first (a) and Pseudo-second (b) order kinetic plots for the adsorption of MB dye onto EGO.

Supplementary Tables

Table S1 Comparison of reaction parameters and properties of GO prepared by different methods

Exfoliation method	Solvents/ Electrolyte	Duration	Yield	Oxygen content	Lateral size	Thickness /Number of layers	Ref.
Chemical oxidation + electrochemical	$(NH_4)_2S_2O_8$/ H_2SO_4	~0.5h	92%	33.7 at.%	>5μm (71%)	1–2 layers (88%)	This work
Electrochemical	NH_4BF_4	>16h	-	36.2 at.%	1μm	1nm	1
Electrochemical	H_2SO_4	~1.5h	-	~20 at.%	-	3-5nm	2
Electrochemical	$(NH_4)_2NO_3$/ H_2SO_4	24-25h	-	24.6 at.%	0.5-2.5μm	2–4 layers	3
Electrochemical	H_2SO_4	0.5-1h	96%	29.2 at.%	<1μm (~80%)	1–3 layers (86%)	4
Electrochemical	$(NH_4)_2SO_4$	~2.4h	>80%	28.3 at.%	0.5-2.5μm (85%)	1–4 layers (80%)	5
Brodie's	fNA/$KClO_3$	3-4d	-	31.6 at.%	-	-	6
Brodie's	fNA/NaCl	3-5d	-	27.8 at.%	-	-	7
Staudenmaier's	fNA/H_2SO_4/ $NaClO_3$	1-10d	-	25.7 at.%	-	-	8
Hummers'	$KMnO_4$/$NaNO_3$ /H_2SO_4	2h	40%	25.6-32.3 at.%	-	-	9
Hummers'	$KMnO_4$//H_3PO_4 /H_2SO_4	1-2d	-	-	1.5-2.0μm	200-300nm	10
Improved Hummers'	$KMnO_4$//H_3PO_4 /H_2SO_4 /$Ba(OH)_2$	5h	-	>10 at.%	-	-	10
Improved Hummers'	$KMnO_4$/K_2FeO_4 /H_2SO_4	5h	84.0%	32.1 at.%	<2.5μm	< 2nm	11
Improved Hummers'	$KMnO_4$/H_2O_2 /H_2SO_4	>2h	-	24.3 at.%	2μm	-	12

Note: fNA (fuming nitric acid).

Table S2 Comparison of the adsorption capacities of MB with various reported adsorbents

Absorbent Material	Adsorption capacity (mg g^{-1})	Ref.
GO	358.3	This work
GO	240.7	13
GO	1.9	14
GO	350.0	15
activated carbon	3.3	15
CMC/kC/AMMT composite beads	10.8	16
GO regenerated cellulose	78.5	17
CMC/Chitosan/GO nanocomposite	122.1	18
Carboxymethyl sago pulp immobilized sago waste hydrogel beads	158.0	19
CMC/acrylic acid/acrylamide/GO hydrogels	133.3	20
GO/humic acid	59.0	21
Carboxymethyl cellulose/carboxylated GO	180.3	22
poly(glycerol sebacate)/chitosan/GO	178.0	23

Note: CMC (carboxymethyl cellulose), kC (k-carrageenan), AMMT (activated montmorillonite).

Table S3 Parameters of Adsorption Isotherms from Langmuir and Freundlich Models of MB dye onto EGO

T/K	Langmuir model			Freundlich model		
	q_m (mg g^{-1})	K_L	R^2	n	K_F	R^2
298	361.0	15.3894	1	349.7	358.9	0.6942

Table S4 Kinetic parameters obtained from pseudo-first order and pseudo-second order model for adsorption of MB dye onto EGO

T/K	Pseudo-first order			Pseudo-second order		
	q_e (mg g^{-1})	k_1	R^2	q_e (mg/g)	k_2	R^2
298	348.4	2.9895	0.8044	366.3	0.0004	0.9990

References:

1 M. Komoda and Y. Nishina, *Electrochim. Acta*, 2022, **430**, 141087.

2 H. Hashimoto, Y. Muramatsu, Y. Nishina and H. Asoh, *Electrochem. commun.*, 2019, **104**, 106475.

3 Z. Ji, M. Perez-Page, J. Chen, R. G. Rodriguez, R. Cai, S. J. Haigh and S. M. Holmes, *Energy*, 2021, **226**, 120318.

4 S. Pei, Q. Wei, K. Huang, H.-M. Cheng and W. Ren, *Nat. Commun.*, 2018, **9**, 145.

5 K. Parvez, R. A. Rincón, N.-E. Weber, K. C. Cha and S. S. Venkataraman, ChemComm, 2016, **52**, 5714-5717.

6 B. C. Brodie, *Philos. Trans. R. Soc. Lond.*, 1859, **149**, 249-259.

7 H.-K. Jeong, Y. P. Lee, R. J. W. E. Lahaye, M.-H. Park, K. H. An, I. J. Kim, C.-W. Yang, C. Y. Park, R. S. Ruoff and Y. H. Lee, *J. Am. Chem. Soc.*, 2008, **130**, 1362-1366.

8 L. Staudenmaier, *Berichte der deutschen chemischen Gesellschaft*, 1898, **31**, 1481-1487.

9 W. S. Hummers and R. E. Offeman, *J. Am. Chem. Soc.*, 1958, **80**, 1339.

10 A. S. Nimbalkar, S. K. Tiwari, S. Kyu Ha and C. Kook Hong, *Mater. Today Proc.*, 2020, **21**, 1749-1754.

11 H. Yu, B. Zhang, C. Bulin, R. Li and R. Xing, *Sci. Rep.*, 2016, **6**, 36143.

12 R. Khan, K. Miyagawa, A. Bianco and Y. Nishina, *Appl. Mater. Today*, 2021, **24**, 101120.

13 Y. Li, Q. Du, T. Liu, X. Peng, J. Wang, J. Sun, Y. Wang, S. Wu, Z. Wang, Y. Xia and L. Xia, *Chem Eng Res Des*, 2013, **91**, 361-368.

14 W. Zhang, C. Zhou, W. Zhou, A. Lei, Q. Zhang, Q. Wan and B. Zou, *Bull Environ Contam Toxicol*, 2011, **87**, 86.

15 P. Bradder, S. K. Ling, S. Wang and S. Liu, *J. Chem. Eng. Data*, 2011, **56**, 138-141.

16 C. Liu, A. M. Omer and X. Ouyang, *Int. J. Biol. Macromol.*, 2018, **106**, 823-833.

17 F. Ren, Z. Li, W.-Z. Tan, X.-H. Liu, Z.-F. Sun, P.-G. Ren and D.-X. Yan, *J Colloid Interface Sci*, 2018, **532**, 58-67.

18 K. Kaur, R. Jindal and Meenu, *Carbohydr. Polym.*, 2019, **225**, 115245.

19 N. A. Dahlan, L. W. Lee, J. Pushpamalar and S. L. Ng, *Int J Environ Sci Te*, 2019, **16**, 2047-2058.

20 H. Dai, Y. Zhang, L. Ma, H. Zhang and H. Huang, *Carbohydr. Polym.*, 2019, **215**, 366-376.

21 D. Li, T. Hua, J. Yuan and F. Xu, *Colloids Surf. A Physicochem. Eng. Asp.*, 2021, **627**, 127171.

22 A. S. Eltaweil, G. S. Elgarhy, G. M. El-Subruiti and A. M. Omer, *Int. J. Biol. Macromol.*, 2020, **154**, 307-18.

23 M. Rostamian, H. Hosseini, V. Fakhri, P. Y. Talouki, M. Farahani, A. J. Gharehtzpeh, V. Goodarzi and C.-H. Su, *Chemosphere*, 2022, **289**, 133219.